Desalination and Water Treatment
www.deswater.com

doi: 10.5004/dwt.2023.29806

304 (2023) 150–161
August

Study on the adsorption performance of steel slag and manganese slag composite materials for lead

Canhua Li[a,b,*], Shuxian Wei[a], Zimu Li[a], Minghui Li[a], Yuhong Zha[a]

[a]*School of Metallurgical Engineering, Anhui University of Technology, Ma'anshan City, Anhui Province, China, Tel.: 18162347179; email: licanhua1979@163.com (C. Li), Tel.: 15385966962; email: wsx1983246954@163.com (S. Wei), Tel.: 13856277356; email: lizimu199803@163.com (Z. Li), Tel.: 18956937970; email: 3503522510@qq.com (M. Li), Tel.: 15240067228; email: 1292945246@qq.com (Y. Zha)*

[b]*Science and Technology Entrepreneurship Service Center, Xuancheng Economic Development Zone, Xuancheng City, Anhui Province, China*

Received 15 December 2022; Accepted 20 July 2023

ABSTRACT

The adsorption properties of Pb^{2+} aqueous solution were studied by means of laboratory-prepared composite particles from steel slag (called SS) and manganese slag (called MS). The effects of the mixing ratio, experimental temperature and adsorption time of the particles on Pb^{2+} were investigated. The isothermal adsorption model of Pb^{2+} and the characterization results were also discussed. Results showed that temperature had little influence on the adsorption process of Pb^{2+}. In the initial solution with Pb^{2+} concentration of 500 mg/L, the best adsorption effect could be achieved when the dosage of particles was 1.0 g. The Pb^{2+} removal efficiency was high when the stirring speed was in the range of 100–300 rpm and the initial solution pH was in the range of 7–9 in the adsorption system. The initial concentration with adsorption equilibrium time of 25 min was 300 mg/L. The adsorption process of the particles fits the Langmuir ISO-temperature model. The maximum saturated adsorption value was 69.93 mg/g.

Keywords: Steel slag; Manganese slag; Lead ion; Adsorption; Thermodynamic model

1. Introduction

The large amount of industrial wastewater containing heavy metals is causing serious environment problems [1]. Lead is one of the most toxic heavy metals. Lead pollution cannot be degraded by microorganisms. It accumulates and easily converts into more toxic methyl compounds [2,3]. Passive plant absorption poses a serious threat to animal feeds and human health [4,5]. The technologies for the treatment of heavy metals include chemical precipitation, biofilm, adsorption and reverse osmosis [6], with the adsorption method have been considered as the most economically promising technologies [7]. Steel slag (called SS) has high specific surface area and high chemical activity, and it can be hydrolyzed to produce $CaO\text{-}SiO_2\text{-}H_2O$ (C-S-H) gel. It is a good adsorbent and has been used for water treatment [7]. It confirmed that Cd, Cu, and Pb can be removed from solutions by the addition of steel slag particles, while the removal efficiency depends on metal type and on the ion interaction, concentration, and pH of precipitation of each metal [8]. However, most studies have not solved the problem of solid–liquid separation after the adsorption of steel slag. As a result, the steel slag after adsorption of heavy metal ion becomes a secondary pollution sludge that must be treated.

The specific surface area of manganese slag is also large. A report indicated the removal rate reached 95.47% by synthetic zeolite sorbent from electrolytic manganese slag [9].

* Corresponding author.

Electrolytic manganese residue (EMR) was thermally activated with calcite to prepare a silicon-based functionalized adsorbent (C-EMR) for the removal of cadmium and lead [10]. Electrolytic manganese residues (EMRs) modified by NaOH, ultrasonic etching and microwave-assisted heating treatment were used as a novel adsorbent to remove Arsenic(V) [As(V)] from synthetic wastewater, results showed that the maximum adsorption capacity of E-EMRs for As(V) was 23.96 mg/g [11,12]. However, the manganese residue generally requires modification when it used as adsorption of heavy metal ions, and the adsorption performance of heavy metal mainly depends on the increase of active species that can adsorb or oxidize heavy metals on its surface. Therefore, the combination of manganese residue and other solid wastes may be the application direction of manganese residue as adsorbent.

According to the previous studies, because the steel slag has the gelling property, it can be hydrated into CaO-SiO_2-H_2O (C-S-H) gel when it meets water, and can be made into ceramsite ball. This can solve the difficulty of solid residue separation from solution after steel slag adsorption of heavy metal ions. On the other hand, steel slag has the property of high alkaline precipitating heavy metals, while manganese slag has the property of large specific surface area. The adsorbent composite ceramsites can be developed from steel slag and manganese slag. The composite ceramides can not only release OH^- to solidify heavy metal ions, but also separate solid from solution, making the removal process easy and cost saving.

In this paper, the composite ceramics were developed from steel slags and manganese slags, and their adsorption characteristics and thermodynamic model for Pb^{2+} were studied. Results of this study indicate that production of the adsorption of Pb^{2+} with composite ceramics made from steel slags and manganese slags, thus, to broaden the way of solid waste resource utilization and provide a certain theoretical basis for the development of new multi-functional environmental protection materials.

2. Materials and methods

2.1. Raw materials

The steel slags used in the experiments were taken from the converter slag of Liuzhou Iron and Steel Co., Ltd. The manganese slags were obtained from Guangxi CITIC Group. The chemical compositions of the samples were analyzed by X-ray fluorescence spectrometer [7–12], as shown in Table 1. From Table 1, silicon dioxide and calcium oxides are the two major chemical constituents of steel slag, while silica and alumina are the major chemicals of manganese slag. The metal oxides such as CaO and MgO in steel slag can be hydrolyzed to form hydroxides, which makes the solution alkaline. The OH^- in the solution can be precipitated by chemical reaction with the heavy metal Pb^{2+} for easy removal. The acidic oxide SiO_2 contained in steel slag is hydrolyzed to form the cementing substance calcium silicate, which also has strong adsorption effect on heavy metals. The siliceous material and ferric oxide in manganese residue play an important role in the adsorption of lead ions, and the preparation as adsorbent can play a certain role in promoting the adsorption.

2.2. Preparation of the SS-MS composite particles

Preparation of adsorbent: As the specific surface area of steel slag is less, the adsorption effect of single steel slag ceramsite is not good. The experiment shows that the specific surface area of adsorption is greatly improved by adding manganese slag into the composite ceramsite. Therefore, in order to explore the best mixing amount of steel slag and manganese slag, prepare raw materials with different proportions. Steel slag and manganese slag were ground to powders of 48 μm in size by a plate mill, then mixed in different ratios of mass to form mixture samples, as Table 2 shows. During pelletization, we sprayed a proper amount of deionised water to make the powder agglomeration. Then, the particles were placed in a dryer (80°C). This step was followed by the drying treatment, which lasted for 36 h. After the particles were cooled, the particles with a diameter of 3–5 mm were sieved out.

The effect of different ratios of manganese slag on the adsorption rate of lead ions was investigated. The results are shown in Fig. 1.

As shown in Fig. 1, the mixing ratio of steel slag and manganese slag is equal to 10 parts. C_2 has the best adsorption effect on the composite particles because the steel slag and manganese slag have larger specific surface areas. Therefore, the incorporation of manganese slag can accelerate the formation of C-S-H gel in the steel slag hydration

Table 1
Chemical composition of steel slag and manganese slag used in this study (mass %)

	Steel slag	Manganese slag
CaO	42.59	–
SiO_2	17.05	33.63
Fe_2O_3	16.33	19.98
Al_2O_3	10.78	33.38
MgO	5.83	1.16
P_2O_5	1.81	1.20
TiO_2	1.76	1.84
MnO	2.55	5.91

Table 2
Mixing ratios of steel slag and manganese slag

Sample number	Ratio (SS-MS)
A	10:0
B	0:10
C_1	9:1
C_2	8:2
C_3	7:3
C_4	6:4
C_5	5:5
C_6	4:6
C_7	3:7
C_8	2:8
C_9	1:9

product to improve the activity of steel slag [13], thus achieving the best removal effect. With the increase of manganese slag content, the adsorption effect has a tendency of decreasing. When the content in the manganese slag content reaches 100%, the removal rate of Pb^{2+} is only about 50%. This finding shows that the adsorption of Pb^{2+} by the composite particles mainly depends on the alkaline environment of the steel slag. The crystal phase of the SS-MS composite particles is shown by X-ray diffraction (XRD). The Brunauer–Emmett–Teller (BET) surface area of the SS-MS composite particles was 19.01 m^2/g, as measured by nitrogen adsorption and desorption isotherm of the SS-MS composite particle and shown in Fig. 2.

2.3. Preparation of adsorbent and simulated water sample

Preparation of simulated polluted water: A total of 0.160 g lead nitrate (analytically pure, 99.0% purity, provided by Chemical Reagent Co., Ltd., of Sinopharm Group, 52 Ningbo Road, Shanghai, China) was weighed with a precision balance with a one-tenth thousandth scale, then placed in a 1,000 mL volumetric flask and dissolved with

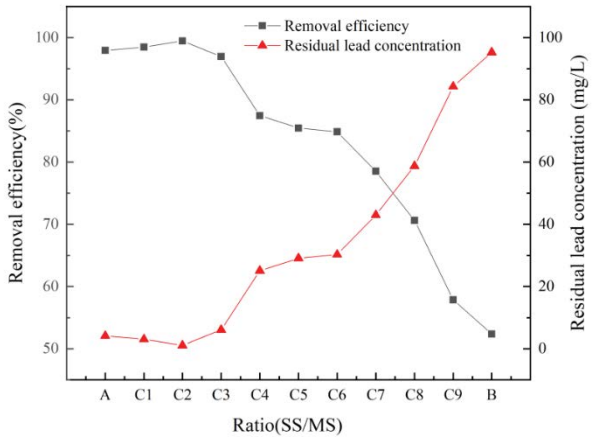

Fig. 1. Effect of SS-MS composite powder in different ratios to lead adsorption.

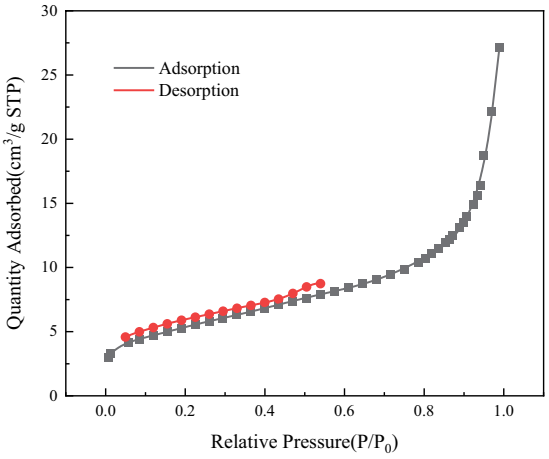

Fig. 2. N_2 adsorption and desorption isotherm of SS-MS composite particles.

10 mL 1.0 M nitric acid (analytically pure, provided by Chemical Reagent Co. Ltd of Sinopharm Group). Deionized water was added to the flask to dilute the solution while shaking. Finally, 1,000 mg/L Pb^{2+} standard solution was obtained as the store solution. Different concentrations were obtained by diluting the store solution.

Selecting the best ingredients for particles: In order to explore which particles prepared with different mixing amounts of steel slag and manganese slag have the best adsorption effect on lead ions in lead standard solution, 1.0 g of *A*, *B*, C_1, C_2, C_3, C_4, C_5, C_6, C_7, C_8, and C_9 particles were taken respectively, and placed in a 100 mL beaker with 100 mg/L lead standard solution, respectively. The adsorption temperature was 25°C, stirring speed was 300r/min and adsorption time was 30 min. At 30 min, the pulp was filtered by filter paper and the lead ion concentration was detected by ICP-AES. The concentrations of Pb^{2+} in the leaching solutions were determined by inductively coupled plasma atomic emission spectroscopy (ICP-AES).

The lead removal rate can be determined by:

$$\eta = \frac{(c_0 - c_e)}{c_0} \times 100\% \quad (1)$$

where η is the lead removal percentage, %; c_0 is the initial concentration of Pb^{2+} in the solution, mg/L; c_e is the concentration of Pb^{2+} after removing for a certain minutes, mg/L.

3. Results and discussion

3.1. Component analysis of steel slag and manganese slag

In order to further understand the mineral composition of steel slag and manganese slag, the mineral composition analysis was carried out by XRD (D8 ADVANCE) under the Cu Ka radiation filtered by Ni, and the results are shown in Fig. 3.

Fig. 3a shows that the diffraction peaks of steel slag are irregular, sharp, and numerous, indicating its complex composition. The main mineral identified was a silicic acid compound, which is consistent with XRF detection results. Fig. 3b displays the analysis of the phase diagram of manganese slag, combined with its main chemical components. The diffraction peaks are irregular with many miscellaneous peaks, but there are a few sharp and high-intensity peaks, indicating the complexity of the composition, with large amounts of quartz and gypsum present. BET specific surface area tests were conducted to obtain relative characterization data for steel slag and manganese slag, and the results are presented in Table 2. Adsorption–desorption isotherms for steel slag and manganese slag are shown in Fig. 4 to investigate their respective adsorption capacities.

From Table 3 the BET test results show that the specific surface area of steel slag is 5.7951 m^2/g, indicating that steel slag powder has a certain adsorption capacity. As can be seen from Table 2, the specific surface area of manganese slag is 19.002 m^2/g, and the pore volume is 0.04 cm^3/g, indicating that manganese slag has an efficient adsorption capacity. According to the adsorption–desorption curve of steel slag powder (Fig. 4a), the two curves basically coincide, which accords with the type II isotherm defined by the

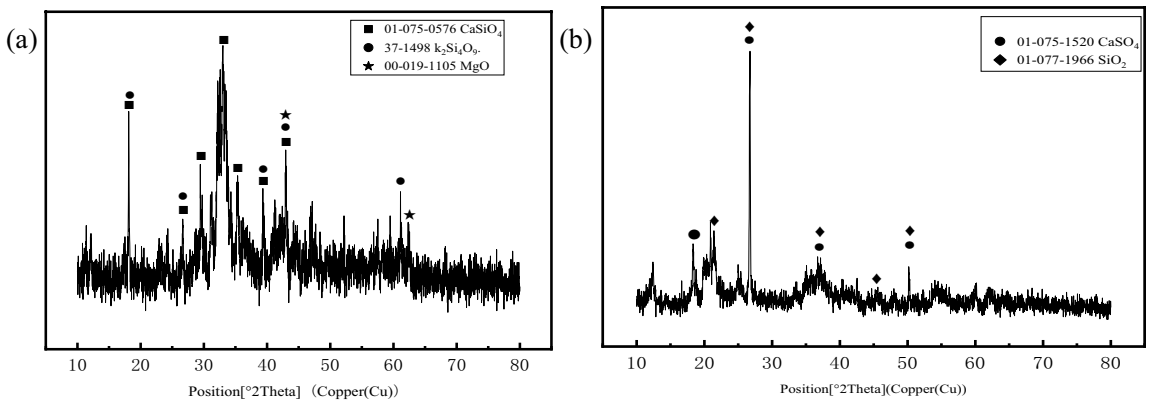

Fig. 3. X-ray diffraction patterns of steel slag and manganese slag.

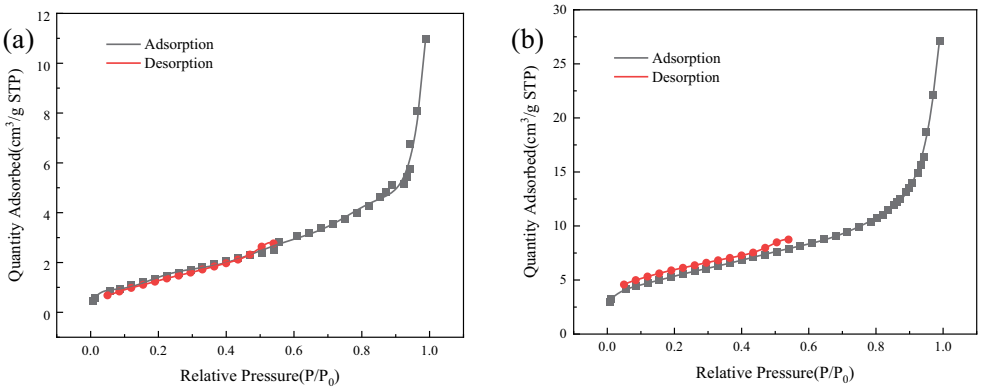

Fig. 4. Adsorption–desorption curves of steel slag powder and manganese slag powder.

Table 3
Brunauer–Emmett–Teller detailed data of steel slag and manganese slag

	Steel slag	Manganese slag
Specific surface area, m^2/g	5.7951	19.002
Density, g/cm^3	1.000	1.000
Volume of pore, cm^3/g	0.017	0.040

International Society for Theoretical and Applied Chemistry (IUPAC), indicating that steel slag adsorption is a single layer adsorption. According to the adsorption–desorption curves of manganese slag (Fig. 4b), the two curves basically coincide, which accords with the type II isotherm defined by the International Society for Theoretical and Applied Chemistry (IUPAC), indicating that the adsorption of manganese slag is also monolayer adsorption.

3.2. Effect of dosage of SS-MS composite particle

First, 0.2, 0.4, 0.6, 0.8, 1.0 and 1.2 g SS-MS composite particles (in which the ratio of steel slag to manganese slag is equal to 8:2) were taken. Then, they were each placed in a 100 mL solution with a lead concentration of 500 mg/L (pH = 6.5). After 30 min of stirring, the solution was extracted for detection. The results are shown in Fig. 5.

According to the trend of the adsorption efficiency curve in Fig. 5, the lead ions in a 100 mL solution with lead concentration of 500 mg/L are completely adsorbed when the dosage of SS-MS composite particles reaches 1.0 g.

3.3. Effect of pH

The influence of pH on adsorption performance is studied by means of batch equilibrium tests of control variables. We adjust the pH of the simulated water sample with 0.1 mol/L NaOH or 0.1 mol/L HNO_3. Then, 1.0 g of SS-MS composite particles were added separately for 30 min of adsorption, and the lead ion content in the mixed solution was detected by ICP-AES. The results are shown in Fig. 6.

The removal efficiency, and residual lead concentration of SS-MS composite particles in the pH range of 1–9 are shown in Fig. 6. According to the trend of removal efficiency, we found that a large pH corresponds to a strong adsorption capacity, thus allowing us to infer that a highly alkaline aqueous environment helps promote deposition.

3.4. Effect of temperature

A total of 1.0 g of SS-MS composite particles was added to the lead-containing water sample with an initial concentration of 500 mg/L (pH = 8, stirring speed = 300 rpm). The adsorption time was 30 min. The concentration of lead ions

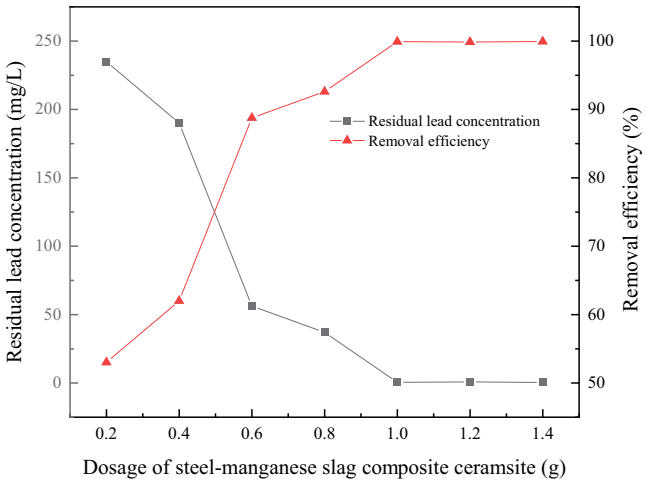

Fig. 5. Effect of dosage of SS-MS composite particles on adsorption of Pb^{2+}.

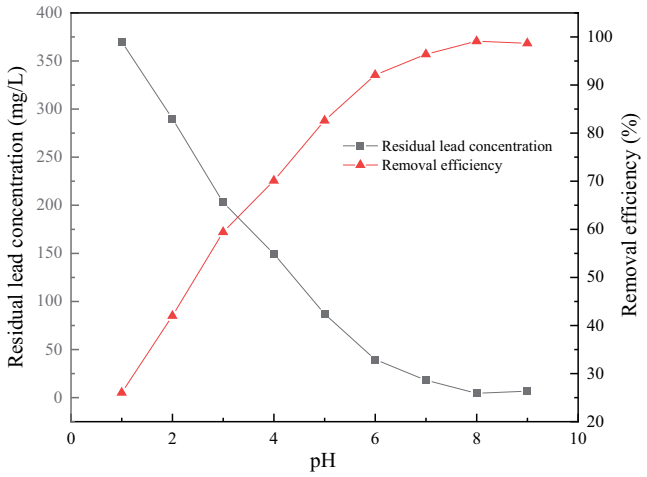

Fig. 6. Effect of pH on adsorption of Pb^{2+}.

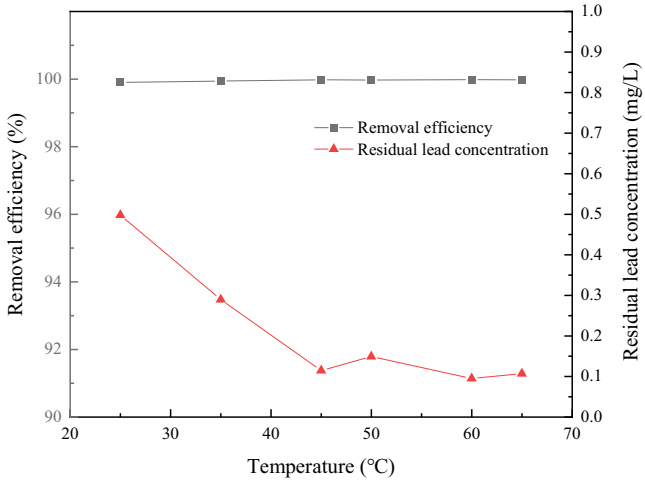

Fig. 7. Effect of reaction temperature on adsorption of Pb^{2+} by SS-MS composite particles.

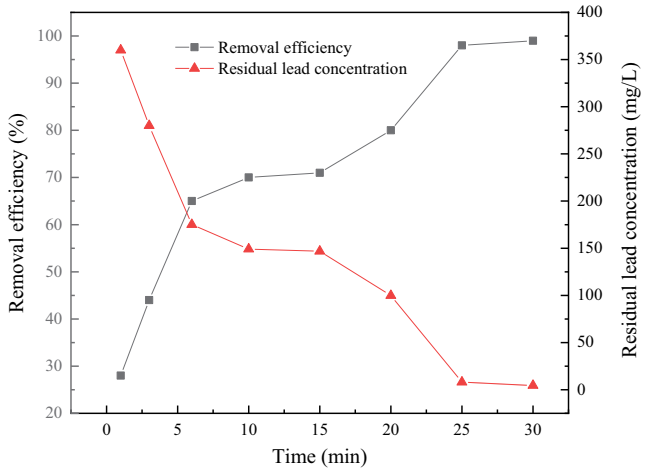

Fig. 8. Effect of adsorption time on Pb^{2+} adsorption by SS-MS composite particles.

in the filtrate was detected by particles on the adsorption effect of lead ions at different temperatures was investigated. The detailed results are shown in Fig. 7.

As shown in Fig. 7, the removal rate of the SS-MS composite particles is about 99%. The reaction temperature has almost no effect on the lead ion adsorption of SS-MS composite particles. As for the residual lead content, although it has a certain degree of change, it can be ignored because the value is very low. Thus, we can conclude that the adsorption process of the SS-MS composite particles has strong adaptability to temperature and good adsorption effect [14,15].

3.5. Effect of adsorption time

The adsorption process of the SS-MS composite particles is complex. In this case, the adsorption process can be divided into different stages according to time [16]. To investigate the process of lead ion adsorption by the SS-MS composite particles, 1.0 g of SS-MS composite particle were added to eight lead-containing water samples with an initial concentration of 500 mg/L (pH = 8), and the adsorption experiment was conducted at room temperature at a stirring speed of 300 rpm. Samples were taken at 1, 3, 6, 10, 15, 20, 25 and 30 min. The results are shown in Fig. 8.

According to the change trend of removal rate with adsorption time in Fig. 8, the process of lead ion adsorption by SS-MS composite particles can be roughly divided into three stages: initial fast adsorption stage, medium slow adsorption stage and equilibrium adsorption stage. At the initial stage of adsorption, the adsorption curve of SS-MS composite particles for lead ions increased significantly. At this time, a large number of free lead ions quickly diffused to the solid–liquid interface, and there were a large number of binding sites were present on the surface of the particle. A small amount of white floccules were formed during the experimental reaction. As time passed, an increasing number of white floccules precipitated. However, the removal efficiency is relatively slow at this stage because the pores on

the surface of the composite particles gradually saturate and lead ions diffuse from the surface to the interior of the composite particles. Finally, at 25 min, the composite particles can completely adsorb lead ions and reach the equilibrium state. The change trend is roughly consistent with the synthesis of the biopolymer, alginate-chitosan composite [17].

3.6. Effect of stirring speed

The stirring speed affects not only the hydrolysis of composite particles but also the contact between lead ions and composite particles. Therefore, the stirring speed is one of the key factors in the investigation of adsorption behaviour. In eight samples with an initial concentration of 500 mg/L (pH = 8), 1.0 g of SS-MS composite particles were added to the samples. The adsorption experiments were conducted at different stirring speeds at room temperature, and the adsorption time was 30 min. The adsorption results are shown in Fig. 9.

As shown in Fig. 9, the adsorption efficiency of the composite particles on lead ions is enhanced with the increase of stirring speed. When the stirring speed is in the range of 100–300 r/min, the adsorption curve of lead ions on the composite particles is steep, because the contact area between lead ions and composite particles can be increased by speeding up the stirring speed, resulting in more binding sites on the surface of composite particles for adsorption in an environment with a higher lead ion concentration [18,19]. At the same time, the agitation speed can accelerate the hydrolysis of the composite particle. At this time, a large amount of C-S-H gel and OH^- can be generated by hydrolysis. The removal rate of Pb^{2+} can be increased by [20]. When the stirring speed is in the range of 300–450 rpm, the adsorption curve of the composite particles is linear, thereby indicating that the residual lead concentration is basically completely absorbed. A fast-stirring speed corresponds to improved adsorption effect of the composite particles on Pb^{2+}. The optimum stirring speed is 300 rpm.

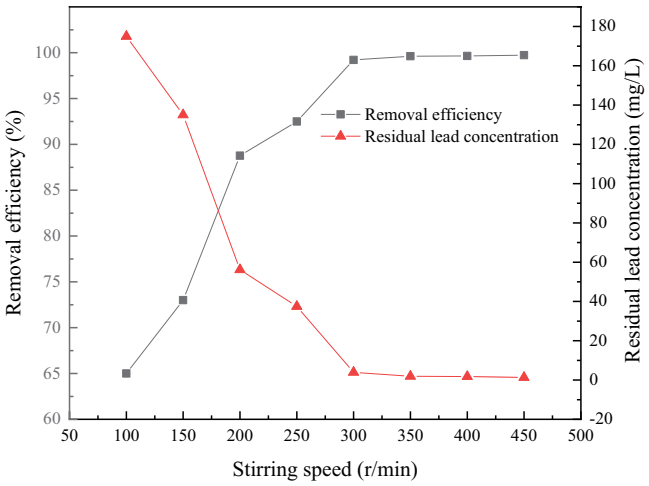

Fig. 9. Effect of stirring speed on adsorption of Pb^{2+} by SS-MS composite particles.

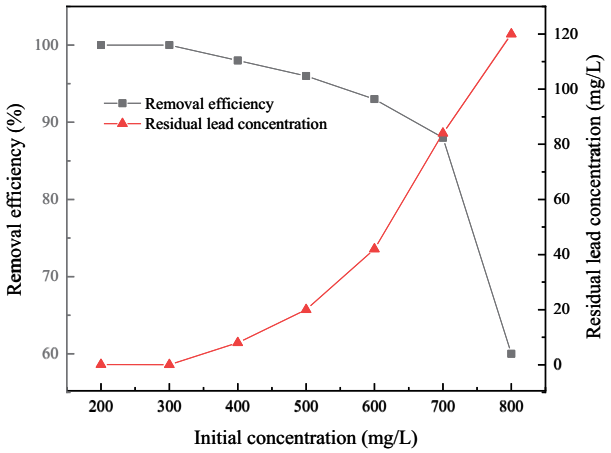

Fig. 10. Effect of initial concentration on Pb^{2+} adsorption by SS-MS composite particles.

3.7. Effect of initial concentration

The initial concentration is of practical significance because it presents the water environment of the adsorbent [21]. At room temperature, 1.0 g of SS-MS composite particles were added to beakers with eight kinds of water samples with different initial lead concentrations (pH = 8). The mixture was then stirred at 300 rpm. The concentration of lead ions in the filtrate was detected by ICP-AES after 0.45 μm membrane filtration. The adsorption results are shown in Fig. 10.

Fig. 10 shows that the removal rate of Pb^{2+} presents a downward trend with the increase in the initial concentration. As a result of the high mobility of Pb^{2+} in the diluted solution, a higher removal rate can be obtained [22,23]. With the increase in the initial concentration, the adsorption capacity of the composite particles tends to be saturated, and all the adsorption sites of Pb^{2+} on the surface of the composite particles are short, resulting in decreased removal rate. The particle tends to be saturated when the initial concentration of particle reaches a fixed value. At this time, further increasing the initial concentration of Pb^{2+} solution will weaken the removal effect of Pb^{2+}.

Considering that SS-MS composite particles are prepared from waste residues, whether the leaching of heavy metals during adsorption meets the US Environmental Protection Agency's (US EPA) standards needs to be confirmed. In the adsorption test group with an initial lead concentration of 200 mg/L, other heavy metal elements were detected through ICP-AES, and the concentrations of Cu^{2+} and Mn^{2+} were 0.9 and 0.01 mg/L, respectively. None of the others were detected. The US EPA secondary maximum contaminant levels for Mn^{2+} are 0.05 mg/L and the US EPA action levels are 1.3 mg/L Cu^{2+} in drinking water [21]. In summary, the absorbed water sample meets the emission standard.

3.8. Removal mechanism of lead by SS-MS composite particle

Lead deposition mechanism of composite particles. The Pb^{2+} absorbing process of the steel slag-manganese slag composite particles is a single-layer adsorption. Thus, its adsorption mainly causes Pb^{2+} to adsorb on the surface of the composite particles by chemical precipitation. Scanning electron microscopy (SEM) surface scanning were used to

investigate the white floc composition generated during the experiment and the effect of lead adsorption on the surface of the composite particles. The entire adsorption process is shown in Fig. 11.

During the deposition process, a large of OH^- was released through ionisation and hydrolysis. Some Pb^{2+} were adsorbed to the surface of the composite particles due to electrostatic action [22]. SEM-EDS detection results confirm the existence of Pb^{2+} on the surface. According to the XRD analysis above, Pb^{2+} combines with OH^- to form white precipitation partly.

In order to further illustrate the adsorption mechanism of Pb^{2+} by SS-MS, as shown in Fig. 12, SEM analysis diagram of sampling of the adsorption of Pb^{2+} by SS-MS at 5, 15, 25 and 40 min.

As shown in Fig. 12, the surface of SS-MS has larger and more pores, and its larger specific surface area can be used for surface adsorption of free Pb^{2+}. In addition, according

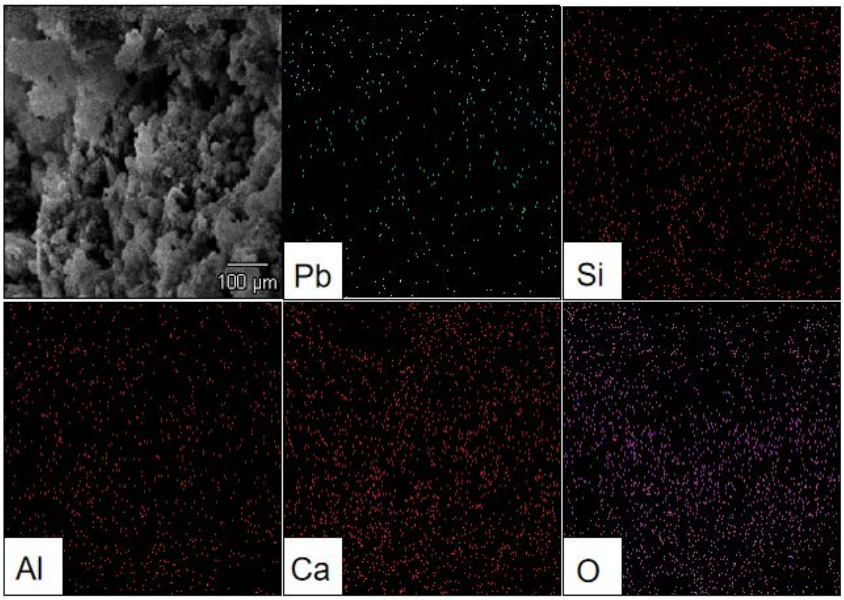

Fig. 11. SS-MS surface scan map after adsorption.

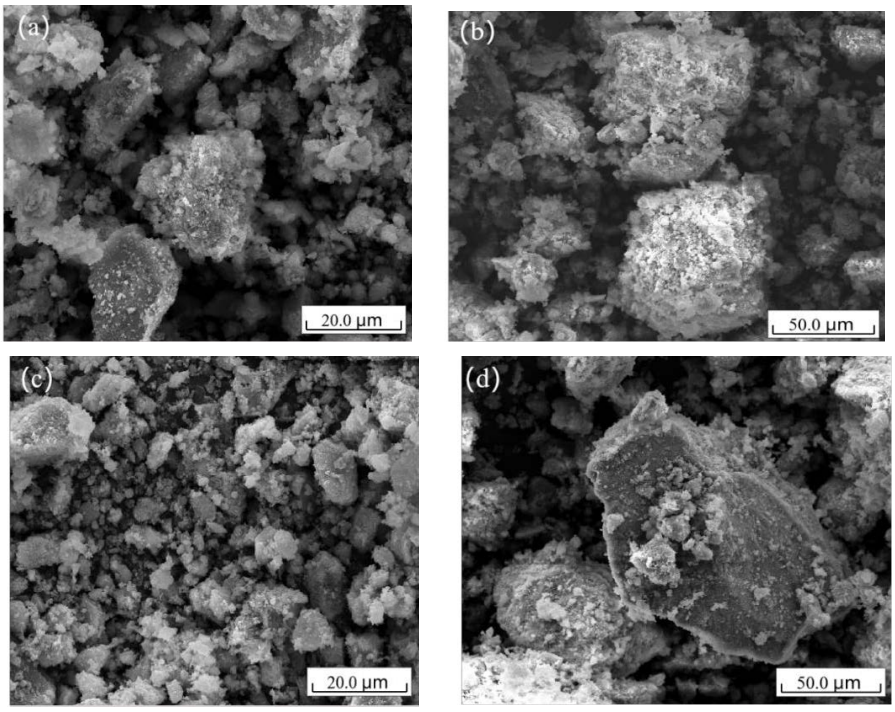

Fig. 12. Scanning electron microscopy diagram of SS-MS adsorb Pb^{2+} at different times.

to Fig. 12a, SS-MS contains a large number of silicates, and SiOH = SiO^- + H^+ reaction can occur, so that SS-MS uses the negative charge generated by surface electrostatic interaction to produce electrostatic adsorption on Pb^{2+}. Meanwhile, according to the above section, the alkalinity released by SS-MS can first neutralize H^+, then precipitate $Pb(OH)_2$ with Pb^{2+}, and inhibit the competitive adsorption of Pb^{2+} by H^+. As shown in Fig. 12a, there are a large number of pores on the surface of SS-MS. At 15 min, there were obvious white flocs formed in clusters. At 25 min, a large number of surface pores of SS-MS were occupied by Pb^{2+}, which were separated and attached to the surface of SS-MS, as shown in Fig. 12c and d.

3.9. Adsorption isotherm experimental study

Under constant temperature conditions, the relationship between the equilibrium adsorption and initial concentration of Pb^{2+} can be represented by the SS-MS and Pb^{2+} isotherm adsorption curve. This curve reflects the adsorption performance of composite particles as absorbents in a reaction and describes the solid adsorption phenomenon in a solution. Fig. 13 displays the relationship between the unit volume of SS-MS and the initial concentration of Pb^{2+} (ranging from 0–1,000 mg/L) at room temperature. The findings indicate that the adsorption capacity of composite particles per unit volume is linearly related to the initial concentration of Pb^{2+} when the initial concentration ranges from 0–700 mg/L. During this phase, the composite particle's surface has ample adsorption sites to completely adsorb Pb^{2+} in the solution. However, as the initial concentration of Pb^{2+} exceeds 700 mg/L, the equilibrium adsorption capacity of composite particles gradually stabilizes, indicating that the adsorption is in a saturated state. At this point, the number of adsorption sites on the surface of composite particles is limited.

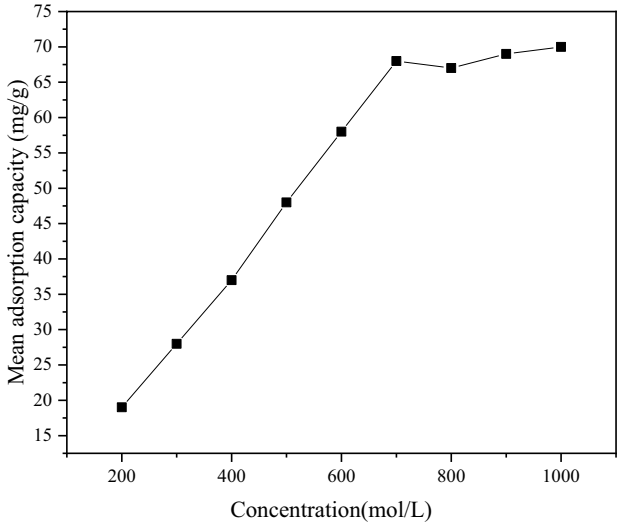

Fig. 13. Isothermal adsorption curve of initial Pb^{2+} concentration.

The adsorption isotherm curve is usually analyzed using the Langmuir isotherm adsorption model and the Freundlich isotherm adsorption model. At room temperature, 1.0 g of SS-MS was placed in 100 mL of lead solution with different initial concentrations. The initial concentrations were 200, 300, 400, 500, 600, 700, 800, 900, and 1,000 mg/L, and the adsorption reaction was carried out during the process. The isotherm adsorption curve of the composite particles can be obtained, and the Langmuir isotherm adsorption line and the Freundlich isotherm adsorption model of Pb^{2+} can be obtained after fitting, as shown in Fig. 14.

As can be seen from the fitting parameters in Table 4, the fitting correlation coefficients R^2 between the composite particles and the Langmuir isothermal model and Freundlich isothermal model during the adsorption of Pb^{2+} are 0.999 and 0.65, respectively, indicating that the adsorption of Pb^{2+} by SS-MS accords with the Langmuir adsorption equation. That is, the adsorption of Pb^{2+} by composite particles belongs to monolayer adsorption, which is consistent with the experimental results of the heat-treated blast furnace slag curing lead experiment [23,24]. In addition, the correlation

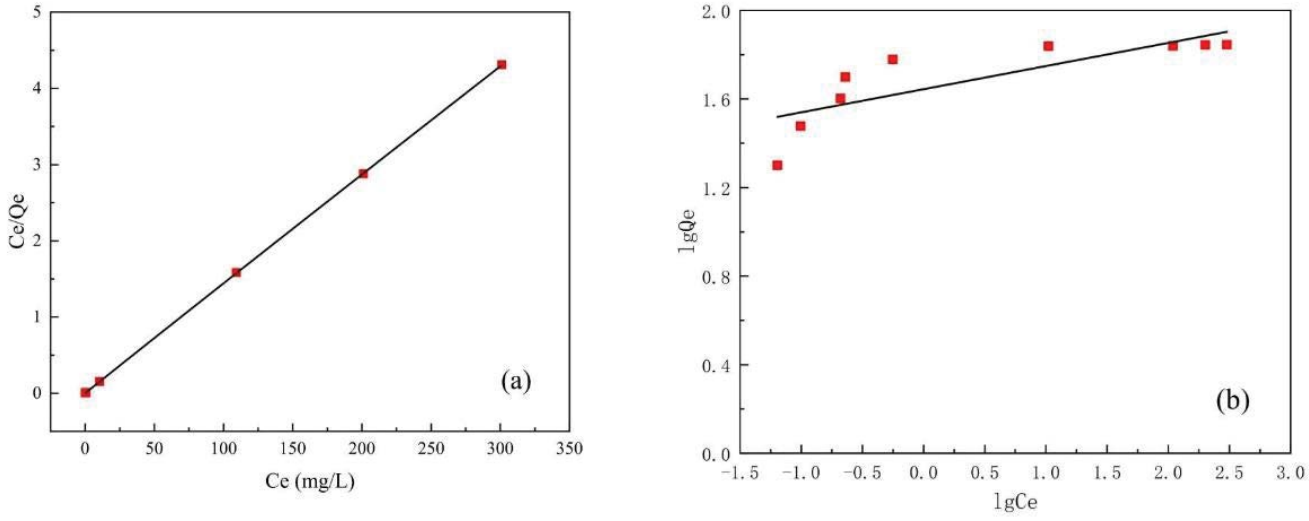

Fig. 14. (a) Langmuir isothermal absorption equation and (b) Freundlich isothermal absorption equation.

coefficients of R_L in the initial concentration range were all between 0 and 1, indicating that the adsorption system promoted the overall adsorption behavior. According to the Langmuir isothermal adsorption model, the theoretical saturated adsorption capacity Q_{max} for Pb^{2+} particles can be calculated to be 69.93 mg/g, which is consistent with the actual saturated adsorption capacity obtained in the experiment of 69.89 mg/g. Shi analyzed the differences in adsorption characteristics and influencing factors of Pb^{2+} between peanut shell biochar and corn cob biochar. Explored the mechanisms of two types of biochar for adsorbing Pb^{2+}. The results showed that the theoretical maximum adsorption amounts of Pb^{2+} on peanut shell biochar and corn cob biochar were 20.85 and 28.51 mg/g, respectively; The adsorption efficiency of this adsorbent is significantly higher than that of this biochar adsorbent [25]. The results show that the adsorption process of Pb^{2+} in water samples by SS-MS is consistent with that by Langmuir isothermal model.

3.10. Experimental study on adsorption kinetics

The process of Pb^{2+} adsorption by SS-MS was analyzed using the Lagergren primary kinetic model and the McKay secondary kinetic model, and the results are presented in Fig. 15 and Table 5. The Lagergren primary kinetic constant k_1 and the McKay secondary kinetic constant k_2 were obtained through fitting, with R^2 values of 0.95822 and 0.97944, respectively. These results suggest that the process of Pb^{2+} adsorption by SS-MS is better described by the McKay secondary kinetic model. This is likely due to the fact that the McKay secondary kinetic model was developed based on the solid-phase adsorption capacity and is more suitable for describing the adsorption process of SS-MS in the presence of saturation sites [26].

3.11. Chemical precipitation action

Since SS-MS is basic, it releases OH^- in aqueous solution, and it can be inferred from the McKay secondary kinetic equation and Langmuir isothermal adsorption model that SS-MS is chemically dominated in the adsorption process. Therefore, when examining the mechanism of SS-MS on Pb^{2+}, chemical precipitation is the primary object of investigation.

3.11.1. SS-MS alkalinity release pattern

Eight portions of 1.0 g SS-MS were weighed and added to eight 500 mL beakers. Then, 200 mL of distilled water was added, and the beakers were shaken at room temperature

Table 4
Parameters in isotherm model

Isotherm model	Parameter	Numerical value
Langmuir model	K_L (L/mg)	4.32
	Q_{max} (mg/mL)	69.93
	R^2	0.999
Freundlich model	K_F (mg/mL)	44.06
	n	9.57
	R^2	0.65

Table 5
Parameters in kinetics model

Dynamical model	Parameters	c_0 = 300 mg/L
Pseudo-first-order	k_1 (min^{-1})	0.43
	q_e (mg/mL)	37.5014
	R^2	0.95822
Pseudo-second-order	k_2 (g/mL·min)	0.59
	q_e (mg/mL)	34.9162
	R^2	0.97944

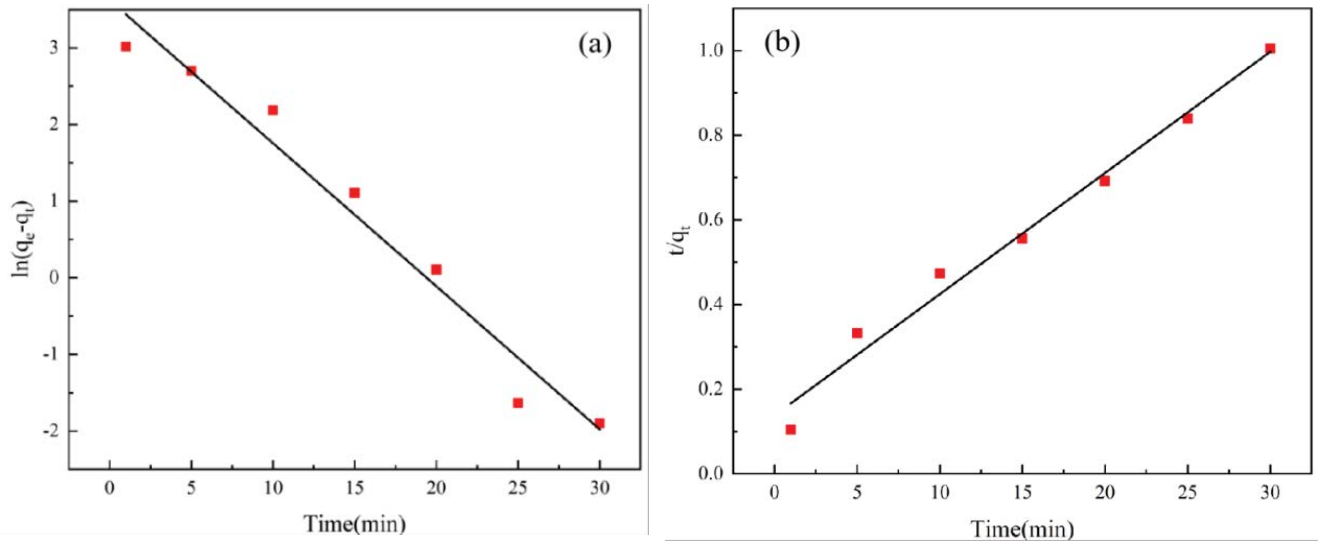

Fig. 15. (a) Lagergren pseudo-first-order and (b) McKay pseudo-second-order.

at a speed of 100 rpm to release alkalinity. The alkalinity in the supernatant was measured at 5, 10, 15, 20, 25, 30, 35, and 40 min, and the alkalinity release curve over time was plotted. The results of the composite particle dealkalization test are presented in Fig. 16.

From Fig. 16, it is clear that SS-MS is releasing alkalinity gradually with the increase of time. From the graph of pH change, it is obvious that the slope of the change line is the largest at 10–15 min, indicating that SS-MS releases alkalinity to the strongest extent at this time, after which the release rate slows down. After 35 min, the pH value of the solution in which SS-MS was located was basically maintained at about 10.3, and the alkalinity level reached equilibrium. The main hydrolysis reactions that occurred during this process were as follows:

$$2\left(2CaO\cdot SiO_2\right)+4H_2O\rightarrow 3CaO\cdot 2SiO_2\cdot 3H_2O+Ca\left(OH\right)_2 \quad (I)$$

$$3\left(3CaO\cdot SiO_2\right)+6H_2O\rightarrow 3CaO\cdot 2SiO_2\cdot 3H_2O+3Ca\left(OH\right)_2 \quad (II)$$

$$2Ca_2SiO_4+4H_2O\rightarrow Ca_3Si_2O_7\cdot 3H_2O+Ca\left(OH\right)_2 \quad (III)$$

$$2Ca_3SiO_5+6H_2O\rightarrow Ca_3Si_2O_7\cdot 3H_2O+3Ca\left(OH\right)_2 \quad (IV)$$

$$Ca\left(OH\right)_2=Ca^{2+}+2OH^- \quad (V)$$

Adsorption is generally divided into chemical precipitation adsorption and physical adsorption. In order to explore the adsorption effect of SS-MS studied in this project, a dealkalization experiment was conducted on the particles, and the dealkalized particles, composite particles, and individual alkali addition were compared for adsorption.

The total alkalinity of this experiment is calculated according to Eq. (2):

$$\text{Alkalinity (in NaOH, mg/L)} = 40\times 10^{14}\text{–pH} \quad (2)$$

where pH is the pH value of SS-MS in deionized water; 40 is NaOH molar mass, g/mol.

The alkalinity released by SS-MS was calculated according to Eq. (2) based on the variation of pH in Fig. 16. For the sake of simplicity of the comparison experiment of NaOH alone in the next step, the amount of NaOH alone was also calculated, and the detailed calculated values are shown in Table 6.

As shown in Fig. 17, it can be seen that the presence of lead ions in different alkaline environments changes in form. At the stage when NaOH is not added and when a trace amount of NaOH is just added, the lead ions in solution exist in the form of Pb^{2+}, and when the appropriate amount of NaOH is gradually added, the free Pb^{2+} in solution reacts with OH^-, and the theoretical reaction process is as follows.

$$H^+ + OH^- = H_2O \quad (VI)$$

$$Pb^{2+} + OH^- = Pb\left(OH\right)^+ \quad (VII)$$

$$Pb\left(OH\right)^+ + OH^- = Pb\left(OH\right)_{2(s)} \quad (VIII)$$

When there is an excess of OH^-, the following reaction also occurs.

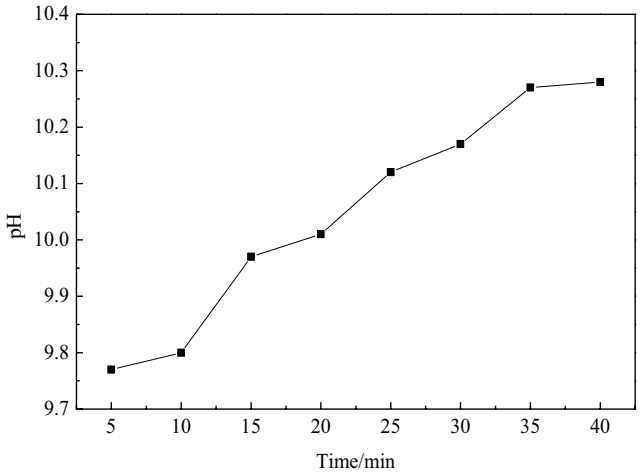

Fig. 16. pH variation rules of SS-MS.

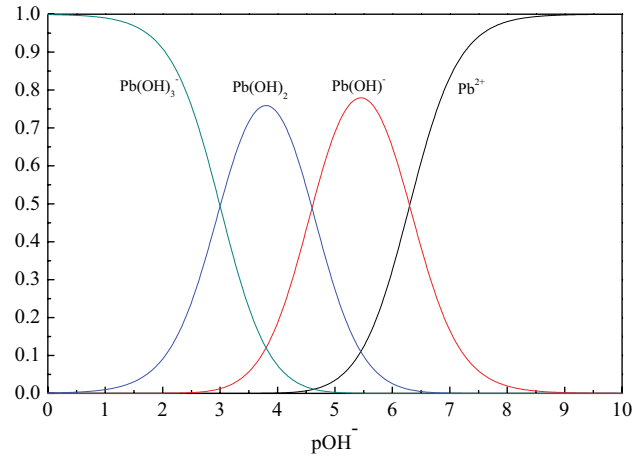

Fig. 17. Formation of lead ions under different alkaline conditions.

Table 6
Dosage of NaOH and the removal quantity of Pb^{2+} in different time

Time (min)	5	10	15	20	25	30	35	40
Release alkalinity (mg)	2.36	2.52	2.97	4.09	5.27	5.92	7.45	7.62
NaOH dosage (mg)	2.36	0.16	0.45	1.12	1.18	0.65	1.53	0.17
Theoretical removal amount of Pb^{2+} (mg)	6.11	6.52	7.22	10.58	13.64	15.32	19.28	19.72

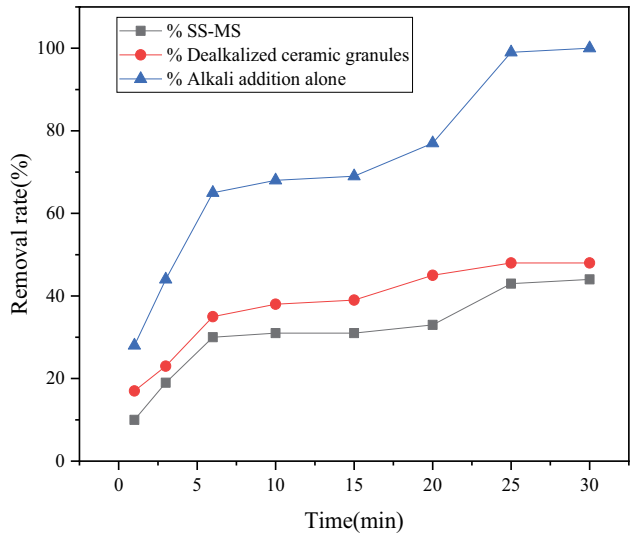

Fig. 18. Absorption curve of SS-MS, and dealkali ceramic granules, and alkali is added separately on Pb^{2+}.

$$Pb(OH)_2 + OH^- = Pb(OH)_3^- \quad \text{(IX)}$$

From Fig. 17, it can be seen that at pH 3~5, lead ions are basically present in solution as amphiphilic precipitate $Pb(OH)_2$, so the pH is controlled in the range of 9~11 in order to make the lead produce precipitates as much as possible. Since the pH value of the configured solution containing lead is 6, OH^- will neutralize H^+ at the beginning of the input of NaOH. Therefore, only reactions (3-11-6), (3-11-7) and (3-11-8) occurred in this test. The alkalinity release of SS-MS is a slow process, and there is no phenomenon of instantaneous release of alkalinity at a certain moment, and the total alkalinity released by SS-MS is not enough to produce $Pb(OH)_2$, so the anti-dissolution phenomenon of (3-11-9) is excluded.

In the actual industrial treatment, the pH was maintained at about 10 by controlling the dosage of SS-MS and the reaction time to prevent the dissolution of $Pb(OH)_2$, resulting in the Pb^{2+} content in the discharge solution exceeding the discharge standard.

3.11.2. Comparison of Pb^{2+} removal effect between SS-MS, de-alkalized particles and alkali addition alone

De-alkalized SS-MS was dried in an oven for 24 h and converted into pellets. In order to investigate the mechanism of SS-MS on Pb^{2+}-containing wastewater, adsorption experiments were carried out using SS-MS, dealkalized pellets, and NaOH alone on lead-containing water samples. The results of these experiments are presented in detail in Fig. 18, and the calculation results are summarized in Table 6.

Based on the data presented in Fig. 18, a comparison of the adsorption effect of three different materials in removing Pb^{2+} ions was conducted, and the following order of effectiveness was observed: SS-MS > dealkalized particles > NaOH alone. The fastest adsorption rate of Pb^{2+} was observed within the first 6 min. In the range of 25–35 min, the adsorption rates of all three materials reached equilibrium, with the adsorption rate of SS-MS approaching 100% at 30 min. The adsorption rate of SS-MS was much higher than that of dealkalized particles and alkali alone, and even exceeded the sum of the two. These results suggest that the removal effect of Pb^{2+} by SS-MS is stronger than that of adsorption alone or chemical precipitation alone. It is inferred that a synergistic effect of adsorption–precipitation occurs during the process of Pb^{2+} removal by SS-MS, where the two effects complement and promote each other to achieve optimal removal efficiency.

4. Conclusions

The utilization of steel slag and manganese slag as adsorbents for heavy metal ion adsorption in water treatment has been established. These adsorbents have promising applications in various fields due to their high adsorption efficiency for heavy metal ions. Therefore, steel slag and manganese slag adsorbents hold great potential for future use in the field of heavy metal ion removal.

- SS-MS composite particles with an 8:2 ratio of steel slag and manganese slag have the best adsorption effect on Pb^{2+}. The adsorption efficiency of Pb^{2+} by composite particles has good adaptability to temperature. Under environmental temperature, 1.0 g of SS-MS composite particles adsorb for 25 min at a stirring rate of 300 r/min in a solution with 300 mg/L Pb^{2+} concentration. The removal efficiency can reach 99% theoretically.
- The characterisation results of the Pb^{2+} removal process of the SS-MS composite particles shows that the removal efficiency of the composite particles is mainly caused by OH^- released from hydrolysis and ionisation.
- The adsorption of Pb^{2+} by SS-MS composite particles is monolayer adsorption, which has good agreement with the Langmuir isothermal adsorption model. The maximum saturated adsorption capacity is 69.93 mg/g.
- The preparation of adsorption composite ceramides using steel slag and manganese slag as raw materials has been established as a feasible approach. These composite ceramides are capable of releasing OH^- ions to solidify heavy metal ions and facilitate the separation of solid from solution. This removal process is advantageous due to its simplicity and cost-effectiveness. The steel slag manganese slag adsorbent not only adsorbs heavy metal ions but also enables the recovery of valuable metal elements contained within it. By utilizing this adsorbent for resource recovery, it is possible to reduce environmental pollution and achieve the resource utilization of waste. Furthermore, the granulation ratio of steel slag manganese slag can be modified to explore its application in the treatment of domestic sewage in real-life scenarios.

Acknowledgments

Ethics approval and consent to participate

Not applicable.

Supplementary information

Not applicable.

Availability of data and materials

Not applicable.

Author contribution

Canhua Li: conceptualisation, software, writing—review and editing.Shuxian Wei: writing—review, conceptualisation, software, writing—original draft, validation, investigation and editing. Zimu Li: conceptualisation, methodology, software, writing—original draft, validation, investigation, writing—review and editing. Yuhong Zha: writing—review and editing. Minghui Li: funding acquisition.

Funding

Projects(YJS202110333) supported by Anhui Province University Graduate Scientific Research Project, Projects(202107d06050012) supported by The central government guides local science and technology development projects.

Consent for publication

Not applicable.

Competing interests

The authors declare that they have no competing interests.

References

[1] Z. Barnett-Itzhaki, J. Eaton, I. Hen, T. Berman, Heavy metal concentrations in drinking water in a country heavily reliant on desalination, Environ. Sci. Pollut. Res., 26 (2019) 19991–19996.
[2] M. Bryan, L.B. Baindu, H.Z. Nasser, K.L. Debomoy, Latent consequences of early-life lead (Pb) exposure and the future: addressing the Pb crisis, NeuroToxicology, 68 (2018) 126–132.
[3] P. Chand, Y.B. Pakade, Removal of Pb from water by adsorption on apple pomace: equilibrium, kinetics, and thermodynamics studies, J. Chem., 1 (2013) 47–57.
[4] Z.S. Fu, S.H. Xi, The effects of heavy metals on human metabolism, Toxicol. Mech. Methods, 30 (2019) 167–176.
[5] E. Islam, D. Liu, T.Q. Li, X. Yang, X.F. Jin, Q. Mahmood, S.K. Tian, J.Y. Li, Effect of Pb toxicity on leaf growth, physiology and ultrastructure in the two ecotypes of *Elsholtzia argyi*, J. Hazard. Mater., 154 (2008) 914–926.
[6] W.L. Lian, L. Yang, J. Stephen, W. Shi, R.J. Bian, J.F. Zhen, L.Q. Li, S.D. Shan, G.X. Pan, Utilization of biochar produced from invasive plant species to efficiently adsorb Cd(II) and Pb(II), Bioresour. Technol., 317 (2020) 914–926.
[7] M. Hejna, D. Gottardo, A. Baldi, V. Dell'Orto, F. Cheli, M. Zaninelli, L. Rossi, Review: nutritional ecology of heavy metals, Animal, 12 (2018) 2156–2170.
[8] S. Liang, S.G. Cao, C.R. Liu, Z. Shah, Y. Cui, G.X. Sun, Heavy metal adsorption using structurally preorganized adsorbent, RSC Adv., 10 (2020) 7259–7264.
[9] Z. Lin, J. Li, Y. Luan, W. Dai, Application of algae for heavy metal adsorption: a 20-year meta-analysis, Ecotoxicol. Environ. Saf., 190 (2019) 110089, doi: 10.1016/j.ecoenv.2019.110089.
[10] M.P. Santa Maria, B.D. Hill, J. Kline, Lead (Pb) neurotoxicology and cognition, Appl. Neuropsychol.: Child., 3 (2018) 272–293.
[11] M.Y. Ma, T. Wang, X. Ke, Y.C. Liu, Y.J. Song, X.J. Shang, J. Li, Q.W. Han, A novel slag composite for the adsorption of heavy metals: preparation, characterization and mechanisms, Environ. Res., 216 (2022) 114442, doi: 10.1016/j.envres.2022.114442.
[12] J.R. Lan, Y. Sun, L. Guo, Y.G. Du, D.Y. Du, T.C. Zhang, J. Li, H.P. Ye, Highly efficient removal of As(V) with modified electrolytic manganese residues (M-EMRs) as a novel adsorbent, J. Alloys Compd., 811 (2019) 151973, doi: 10.1016/j.jallcom.2019.151973.
[13] T.J. Medina, S.P. Arredondo, R. Corral, A. Jacobo, R.A. Zárraga, C.A. Rosas, F.G. Cabrera, J.M. Bernal, Microstructure and Pb^{2+} adsorption properties of blast furnace slag and fly ash based geopolymers, Minerals, 10 (2020) 808, doi: 10.3390/min10090808.
[14] P. Chand, Y.B. Pakade, Removal of Pb from water by adsorption on apple pomace: equilibrium, kinetics, and thermodynamics studies, J. Chem., 2013 (2013) 47–57.
[15] F.M. Francisca, D.A. Glatstein, Influence of pH on cadmium, copper, and lead removal from wastewater by steel slag, Desal. Water Treat., 57 (2015) 21610–21618.
[16] W. Shi, H. Li, G. Liao, G. Pei, Y. Lin, Carbon steel slag and stainless-steel slag for removal of arsenic from stimulant and real groundwater, Int. J. Environ. Sci. Technol., 15 (2017) 2337–2348.
[17] M.F. Hamza, N.A. Hamad, D.M. Hamad, M.S. Khalafalla, A.A.-H. Abdel-Rahman, I.F. Zeid, Y.Z. Wei, M.M. Hessien, A. Fouda, W.M. Salem, Synthesis of eco-friendly biopolymer, alginate-chitosan composite to adsorb the heavy metals, Cd(II) and Pb(II) from contaminated effluents, Materials, 14 (2021) 2189, doi: 10.3390/ma14092189.
[18] N.K. Soliman, A.F. Moustafa, Industrial solid waste for heavy metals adsorption features and challenges; a review, J. Mater. Res. Technol., 9 (2020) 10235–10253.
[19] S.-J. Tae, K. Morita, Immobilization of Cr(VI) in stainless steel slag and Cd, As, and Pb in wastewater using blast furnace slag via a hydrothermal treatment, Met. Mater. Int., 23 (2017) 576–581.
[20] T.L. Van, C.T. Bao, K.N.T. Thi, V.T. Xuan, D.N. Dinh, N. Minh-Hiep, T.T.D. Thi, H.N. To, S.L. Hoang, Preparation of cross-linked magnetic chitosan particles from steel slag and shrimp shells for removal of heavy metals, Environ. Technol., 39 (2018) 1745–1752.
[21] L.J. Zhu, W.J. Wang, Q. Jin, Removal of Cr(III) and Cr(VI) in wastewater by steel slag, Multipurpose Util. Mineral Resour., 219 (2019) 103–106.
[22] S.M. Awadh, F.H. Abdulla, Purification of aqueous solutions from Pb(II) by natural bentonite: an empirical study on chemical adsorption, Environ. Earth Sci., 76 (2017) 386–394.
[23] L.P. Xiao, Z. Liu, J.C. Bai, Zn2+ removal mechanism by bentonite-steel slag composite particles, China Coal Soc., 42 (2017) 1005–1012.
[24] Y. Mohammed, S. Kang, Removal of Co(II) and Cr(III) from aqueous solution by graphene nanosheet/δ-MnO_2: batch and column studies, Chem. Eng. Res. Des., 195 (2020) 477–490.
[25] X.L. Shi, Y. An, Z.H. Wang, C. Yang, Y.J. Wang, B.L. Fan, Adsorption characteristics and mechanisms of lead ions on two types of biochar, Nonferrous Met. Eng., 13 (2023) 127–135.
[26] Y. Mohammed, S. Kang, Removal of Co(II) and Cr(III) from aqueous solution by graphene nanosheet/δ-MnO_2: batch and column studies, Chem. Eng. Res. Des., 195 (2020) 477–490.